Poisson's Ratio Induced Radial Inertia Confinement During Dynamic Compression of Hyperelastic Foams

Brett Sanborn[1,*], *Bo* Song[1], *Wei-Yang* Lu[2]

[1]Sandia National Laboratories, 1515 Eubank SE, Albuquerque, New Mexico 87185, USA
[2]Sandia National Laboratories, 7011 East Avenue, Livermore, California 94551, USA

Abstract. Hyperelastic foams have excellent impact energy absorption capability and can experience full recovery following impact loading. Consequently, hyperelastic foams are selected for different applications as shock isolators. Obtaining accurate intrinsic dynamic compressive properties of the hyperelastic foams has become a crucial step in shock isolation design and evaluation. Radial inertia is a key issue in dynamic characterization of soft materials. Radial inertia induced stress in the sample is generally caused by axial acceleration and large deformation applied to a soft specimen. In this study, Poisson's ratio of a typical hyperelastic foam – silicone foam – was experimentally characterized under high strain rate loading and was observed to drastically change across the densification process. A transition in the Poisson's ratio of the silicone foam specimen during dynamic compression generated radial inertia which consequently resulted in additional axial stress in the silicone foam sample. A new analytical method was developed to address the Poisson's ratio-induced radial inertia effects for hyperelastic foams during high rate compression.

1 Introduction

Hyperelastic foams have been extensively used in thermal isolation, vibration reduction, and shock mitigation applications. In such applications, foam materials are subjected to high strain rate loading and large deformations simultaneously. Computational tools and numerical simulation are required for improved shock isolation design and evaluation, which depend on direct experimental input of intrinsic material properties under dynamic loading.

As an important material parameter, Poisson's ratio of foam materials has been observed to be positive, zero, or even negative depending on the cell structure, density, and matrix material [1]. Due to high nonlinearity at large deformation and drastic hardening behavior after densification, Poisson's ratio of foam materials has been found to vary with specimen strain [2-6]. Treated as compressible solids with a constant Poisson's ratio at small deformations, foam materials may approach a nearly incompressible rubbery state when subjected to large deformation into densification. However, Poisson's ratio of foam materials across densification has been rarely characterized in experiments, particularly at high strain rates.

In Kolsky bar experiments, soft materials are subjected to radial inertia while being loaded axially. The radial inertia induces additional axial stress, the amplitude of which depends on specimen geometry, axial strain acceleration, and Poisson's ratio. In the past, the radial-inertia-induced axial stress was analyzed and corrected based on constant Poisson's ratio assumption [7]. However, currently available formulas of radial-inertia-induced stress may not be applicable to soft hyperelastic foams such as silicone foams, which possess variable Poisson's ratio during dynamic compression. This warrants a new theoretical analysis of radial-inertia-induced stress in hyperelastic foams with variable Poisson's ratio.

In this study, Poisson's ratio of a hyperelastic silicone foam was experimentally measured under high rate compressive loading and large deformation into densification. Based on the measured Poisson's ratio, a general radial inertia analysis for a material with a non-constant Poisson's ratio was developed and verified with experiments at high strain rates.

2 Materials and Specimens

A silicone foam with an open-cell structure was used in this study to characterize Poisson's ratio and induced radial inertia effects under large deformation at high strain rates. The cells of the silicone foam were approximately 0.5 mm in size while the density of the foam was 649.1 ± 14.1 kg/m^3. The cylindrical foam specimens for Poisson's ratio characterization had a thickness of 2.85 mm and a diameter of 9.4 mm.

3 Experiments

Poisson's ratio was measured at dynamic strain rates (1000 s^{-1}, 2000 s^{-1}, and 4000 s^{-1}) using a Kolsky compression bar as shown in Fig. 1. The Kolsky

* Corresponding author: bsanbor@sandia.gov

compression bar had a common diameter of 25.4 mm and was made of 7075 aluminum with lengths of 3.7 m and 2.1 m for the incident and transmission bars, respectively. Pulse shaping was used to achieve constant strain rate and dynamic stress equilibrium in the specimen during dynamic compression. Dynamic force equilibrium was verified using quartz crystal force transducers (QCFT) embedded at the specimen ends of the incident and transmission bars [8]

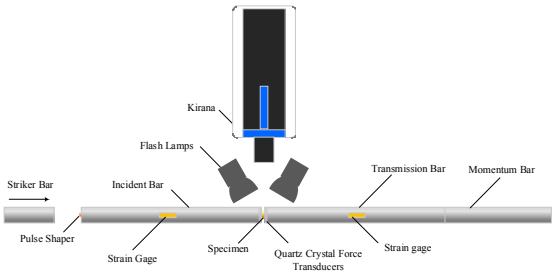

Fig. 1. Kolsky compression bar with imaging to measure Poisson's ratio.

Under stress equilibrium, the transmitted strain history recorded from the transmission bar, ε_t, was used to calculate the engineering stress history in the specimen using the following equation [9],

$$\sigma = \frac{A_B}{A_0} E\varepsilon_t \qquad (1)$$

where A_B and A_0 are the bar and specimen cross-sectional areas, respectively; and E is the bar Young's modulus. Engineering strain rate and strain in the specimen were calculated with the reflected strain history, $\varepsilon_{reflected}$,

$$\dot{\varepsilon} = \frac{-2C_0\varepsilon_{reflected}}{l_0} \qquad (2)$$

$$\varepsilon = \frac{-2C_0}{l_0}\int_o^t \varepsilon_{reflected}\,dt \qquad (3)$$

where C_0 is the bar wave velocity and l_0 is the original specimen length.

Images of the specimen deformation were taken with a high-speed camera at frame rates of 250,000 to 650,000 frames per second depending on the strain rate. High-speed images from a typical dynamic experiment at 2000 s^{-1} are shown in Fig. 2. Both axial and radial engineering strains of the specimen were directly measured from the high-speed images. As shown in Fig. 3, measurements were taken at three locations along the sample thickness to check for uniform deformation. Corresponding axial and radial engineering strains from high-speed images are shown in Fig. 4. In this study, the specimen strain is taken to be positive in compression and negative in tension. Therefore, when the specimen is subjected to axial compression, the axial strain is positive and the radial strain is negative. Although silicone oil was used to lubricate the bar-specimen interfaces, a small amount of barreling in the sample was observed. However, all three radial strain measurements overlapped, indicating that any barreling in the sample had an insignificant effect on the measured radial strain.

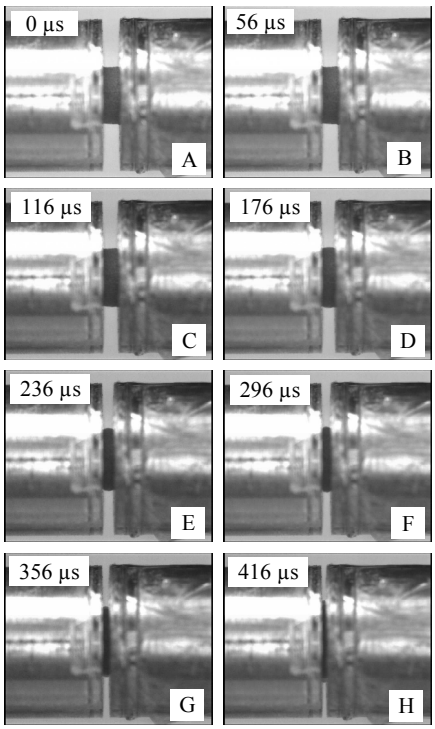

Fig. 2. High-speed images from an experiment at 2000 s^{-1}.

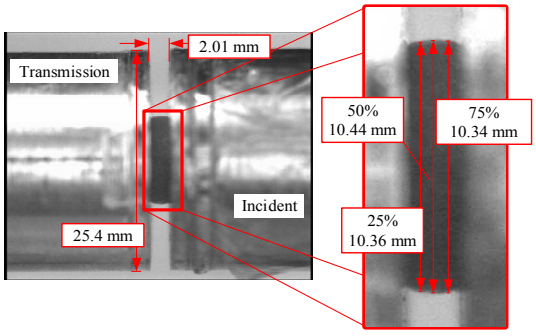

Fig. 3. Example of radial and axial displacement measurements taken at different points on the sample. This image is frame D from Fig. 2.

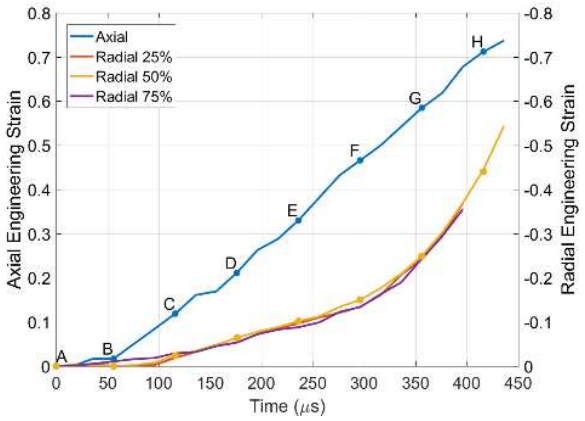

Fig. 4. Axial and radial strain response of silicone foam at 2000 s^{-1}. Letters correspond to time-stamped images from Fig. 2. Radial strains were measured at three locations at approximately 25, 50, and 75% of the specimen length and are correspondingly marked.

4 Experimental Results

After radial and axial strains in the specimen were measured, Poisson's ratio was calculated with the following equation [10, 11],

$$\nu = -\frac{d\varepsilon_r}{d\varepsilon_x} \tag{4}$$

where ε_r and ε_x in Equation (4) are true strains along radial and axial direction, respectively. Considering positive in compression and negative in tension, the true specimen strain, ε, can be calculated from engineering specimen strain, e, with the same equation, regardless of direction,

$$\varepsilon = -\ln(1-e) \tag{5}$$

Using the method described in the previous section, the radial and axial true strains were obtained at three different axial engineering strain rates (1000, 2000, and 4000 s^{-1}) and are plotted in Fig. 5. The radial-axial true strain relationship was observed to be independent of strain rate. In addition, Fig. 5 shows a bilinear relationship between radial-axial true strains, the tangent slopes of which represent Poisson's ratio according to Equation (4). A constant tangent slope represents a constant Poisson's ratio. As shown in Fig. 5, the silicone foam an initial constant (0.21) Poisson's ratio that transitioned to a higher constant Poisson's ratio (0.43) at an approximate axial true strain of 0.75 where the foam material became densified. Fig. 6 shows the Poisson's ratio as a function of axial engineering strain: a constant Poisson's ratio (0.21) was observed when $e_x \leq 0.45$ whereas the Poisson's ratio transitioned to another constant (0.43) when $e_x \geq 0.55$. The transition of Poisson's ratio occurs when $0.45 < e_x < 0.55$. A Boltzmann function was used in this study to describe the Poisson's ratio as a function of axial engineering strain as

$$\nu(e_x) = \frac{\nu_1 - \nu_2}{1+\exp\left(\frac{e_x - e_{x0}}{\delta}\right)} + \nu_2 \tag{6}$$

where ν_1, ν_2, e_{x0}, and δ are Boltzmann fitting constants. The constants used to fit the data in Fig. 5 are shown in Table 1.

Table 1. Fitting constants in Boltzmann function for dynamic Poisson's ratio.

Parameter	Value
ν_1	0.21
ν_2	0.43
e_{x0}	0.525
δ	0.01

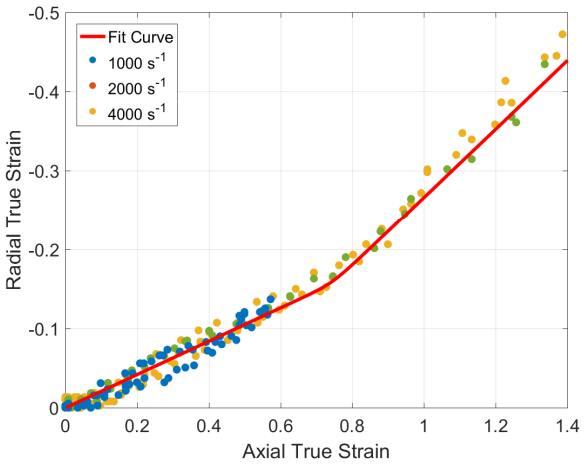

Fig. 5. Radial and axial true strain for all high rate experiments.

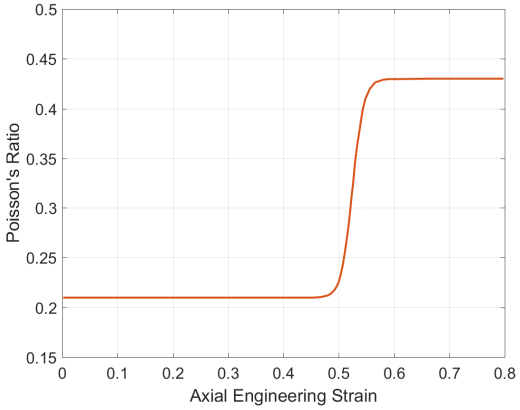

Fig. 6. Stress-strain and Poisson's Ratio relationship for high rate response of foam.

5 Poisson's Ratio-Induced Radial Inertia

Because the Poisson's ratio of the silicone foam transitioned during dynamic loading to a value of 0.43 that approaches near incompressibility, radial inertia effects in the sample must be considered. Radial inertia effects have been observed for soft materials such as rubbers and biological tissues [12]. Radial-inertia-induced confinement resulted in a stress spike in dynamic stress-strain response of such materials along axial loading direction. However, previous formulas used to calculate the radial-inertia-induced stress assumed a constant, and in some cases an incompressible Poisson's ratio. This is not the case for the silicone foam material in this study. As shown in Fig. 6, this drastic change in Poisson's ratio may result in a sudden radial confinement effect in the specimen which in turn adds extra, radial-inertia-induced axial stress to the specimen stress history. Therefore, current methods of calculating the radial-inertia-induced stress cannot be used to calculate the radial-inertia-induced stress in such a hyperelastic foam specimen that exhibits a transition in Poisson's ratio. A new theoretical analysis of Poisson's ratio induced radial inertia effect is thus needed.

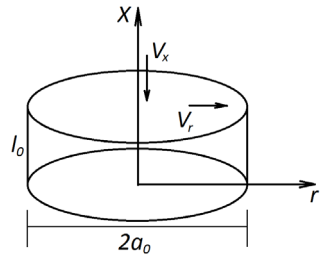

Fig. 7. Coordinate system and nomenclature for compression specimen.

In this study, we consider a cylindrical specimen configuration with initial dimensions of radius, a_0, and length, l_0, for radial inertia analysis, as shown in Fig. 7. An axial compression at velocity $V_x = V_x(t)$ generates a radial expansion with a different velocity, $V_r = V_r(r, t)$. Like the analyses in [7] and [13], mass and momentum conservations in the foam specimen give the following radial-inertia-induced stress in the sample

$$\sigma_r(r,t)=\rho(t)\cdot\frac{a^2(t)-r^2(t)}{2\left(1-e_x(t)\right)}\cdot\begin{bmatrix}\nu(t)\ddot{e}_x(t)+\\ \nu(t)\cdot\left(\nu(t)+1\right)\dfrac{\dot{e}_x^2(t)}{1-e_x(t)}\\ +\dfrac{d\nu(e_x)}{de_x}\dot{e}_x^2(t)\end{bmatrix} \quad (7)$$

where $r(t)$ is any point along the radius; $a(t)$ and $\rho(t)$ are instantaneous radius and density of the specimen, respectively. These three variables can be calculated with the following equations,

$$r(t)=r_0\cdot\exp\left(\int_0^{e_x}\frac{\nu}{1-e_x}de_x\right) \quad (8)$$

$$a(t)=a_0\cdot\exp\left(\int_0^{e_x}\frac{\nu}{1-e_x}de_x\right) \quad (9)$$

$$\rho(t)=\rho_0\cdot\exp\left(\int_0^{e_x}\frac{1-2\nu}{1-e_x}de_x\right) \quad (10)$$

Substituting Equations (6), (8) – (10) into Equation (7) yields

$$\sigma_r(r_0,t)=\rho_0\cdot\frac{a_0^2-r_0^2}{2\left(1-e_x(t)\right)^2}\cdot\begin{bmatrix}\ddot{e}_x(t)\cdot\left(\nu_2+\dfrac{\nu_1-\nu_2}{1+\exp\left(\frac{e_x(t)-e_{x0}}{\delta}\right)}\right)+\\ \dot{e}_x^2(t)\cdot\dfrac{\nu_2-\nu_1}{\delta}\cdot\\ \dfrac{\exp\left(\frac{e_x(t)-e_{x0}}{\delta}\right)}{\left(1+\exp\left(\frac{e_x(t)-e_{x0}}{\delta}\right)\right)^2}\\ +\left(\nu_2+\dfrac{\nu_1-\nu_2}{1+\exp\left(\frac{e_x(t)-e_{x0}}{\delta}\right)}\right)\cdot\\ \left(1+\nu_2+\dfrac{\nu_1-\nu_2}{1+\exp\left(\frac{e_x(t)-e_{x0}}{\delta}\right)}\right)\cdot\\ \dfrac{\dot{e}_x^2(t)}{1-e_x(t)}\end{bmatrix} \quad (11)$$

The average radial-inertia-induced stress is thus calculated as

$$\bar{\sigma}_r(t)=\frac{\rho_0\cdot a_0^2}{4\left(1-e_x(t)\right)^2}\cdot\begin{bmatrix}\ddot{e}_x(t)\cdot\left(\nu_2+\dfrac{\nu_1-\nu_2}{1+\exp\left(\frac{e_x(t)-e_{x0}}{\delta}\right)}\right)+\\ \dot{e}_x^2(t)\cdot\dfrac{\nu_2-\nu_1}{\delta}\cdot\\ \dfrac{\exp\left(\frac{e_x(t)-e_{x0}}{\delta}\right)}{\left(1+\exp\left(\frac{e_x(t)-e_{x0}}{\delta}\right)\right)^2}\\ +\left(\nu_2+\dfrac{\nu_1-\nu_2}{1+\exp\left(\frac{e_x(t)-e_{x0}}{\delta}\right)}\right)\cdot\\ \left(1+\nu_2+\dfrac{\nu_1-\nu_2}{1+\exp\left(\frac{e_x(t)-e_{x0}}{\delta}\right)}\right)\cdot\\ \dfrac{\dot{e}_x^2(t)}{1-e_x(t)}\end{bmatrix} \quad (12)$$

Now we consider a silicone foam specimen which had a density of ρ_0 = 649.1 kg/m^3 and a diameter of 15 mm (a_0 = 7.5 mm). The Poisson's ratio of the foam specimen follows the Boltzmann function (Equation (6)) with the constants listed in Table 1. For a dynamic compression test with a maximum constant strain rate of approximately 4000 s^{-1} and a ramp rise time of about 40 μs, the average radial-inertia-induced stress was

calculated with Equation (12) and plotted as a function of engineering strain as shown in Fig. 8. According to Equation (7), the radial inertia was induced by three mechanisms : 1) strain acceleration (the first term in the bracket in Equation (7) ; 2) large deformation (the second term in the bracket in Equation (7) ; and 3) the change of Poisson's ratio (the third term in the bracket in Equation (7). Fig. 8 shows the radial-inertia-induced axial stresses by the three individual mechanisms and the total amount of the radial-inertia-induced stress. The radial inertia caused by the change of Poisson's ratio generates an additional axial stress peak of 3.57 MPa in magnitude. The peak-valley value of the spike was measured as 2.85 MPa, as marked in Fig. 8. An experimental engineering stress-strain curve at a similar strain-rate condition of 4000 s^{-1} is shown in Fig. 9. The stress-strain curve has a noticeable bump in the response at an engineering strain of approximately 0.53 with a peak-valley value of 3.36 MPa close to the prediction shown in Fig. 8. Similar behavior was observed in the stress-strain curves of 1000 and 2000 s^{-1}. This indicates that Equation (12) can be used along with an experimentally obtained Poisson's ratio (Fig. 6) to predict the magnitude and position of the radial-inertia-induced stress spike at high strain rates for soft, hyperelastic materials such as silicone foam.

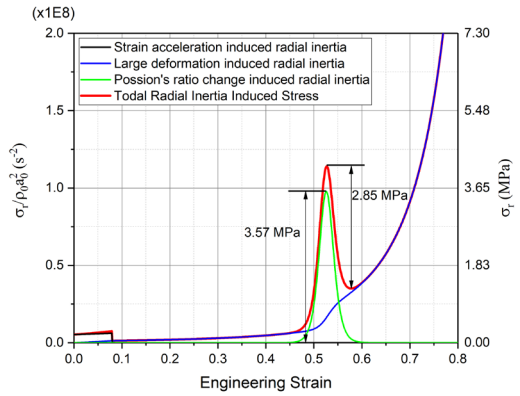

Fig. 8. Analytical prediction of radial-inertia-induced stress of compressible silicone foam sample with transitioning Poisson's Ratio for strain rate of 4000 s^{-1}.

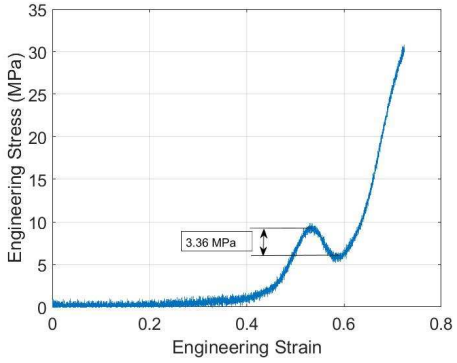

Fig. 9. Experimental engineering stress-strain curve at 4000 s^{-1} showing a bump in the stress-strain curve like the predicted radial-inertia-induced stress.

6 Conclusion

In this study, hyperelastic silicone foam was experimentally characterized in terms of Poisson's ratio and stress-strain response under high rate compression to large deformations. The Poisson's ratio was measured using a high speed camera and was observed to transition from being compressible at small deformation to being nearly incompressible at large deformation. This transition in Poisson's ratio during high strain rate deformation leads to significant radial inertia during dynamic compression. The Poisson's ratio-induced radial inertia consequently results in an extra axial stress in the sample. A new formulation was thus derived to calculate the radial-inertia-induced stress with transitioning Poisson's ratio for such materials. The predicted radial-inertia-induced stress was found to be on a similar magnitude to experimental measurement under similar conditions of strain rate history. The same formulation can also be used to numerically correct the radial-inertia-induced stress due to the change of Poisson's ratio.

Sandia National Laboratories is a multimission laboratory managed and operated by National Technology and Engineering Solutions of Sandia, LLC, a wholly owned subsidiary of Honeywell International, Inc., for the U.S. Department of Energy's National Nuclear Security Administration under contract DE-NA0003525.

References

1. P. Pastorino, F. Scarpa, S. Patsias, J.R. Yates. S.J. Haake, M. Ruzzene. Phys. Status. Solidi. B, **244** (2007)
2. B. M. Patterson, N.L. Cordes, K. Henderson, J.J. Williams, T. Stannard, S. S. Singh, A. R. Ovejero, X. Xiao, M. Robinson, N. Chawla. J. Mater. Sci., **51** (2016)
3. M.F. Beatty, D.O. Stalnaker. J. Appl. Mech., **53** (1986)
4. W.H. El-Ratal, P.K. Mallick. J. Eng. Mater. Technol., **118** (1996)
5. L. Goglio, J Manfredini Vassoler, M. Peroni, Materialwiss, Werkstofftech, **42** (2011)
6. J.A. Rinde J. Appl. Polym. Sci., **14** (1970)
7. T.L. Warren and M.J. Forrestal. Exp. Mech., **50** (2010)
8. D. Casem, T. Weerasooirya, P. Moy. Exp. Mech., **45** (2005)
9. W. Chen, B. Song. Split Hopkinson (Kolsky) bar. Design, testing and applications (2011)
10. K.L. Alderson, A. Alderson, K.E. Evans. J. Strain Anal. Eng. Des., **32** (1997)
11. C.W. Smith, R.J. Wootton, K.E. Evans., Exp. Mech., **39** (1999)
12. B. Song, W. Chen, Y. Ge, T. Weerasooriya. J. Biomech., **40** (2007)
13. C.K.H. Dharan, F.E. Hauser, Exp. Mech., **10** (1970)